




First-principles calculations of lattice thermal conductivity in Tl_3VSe_4 : Uncertainties from different approaches of force constants

Zhi Li ¹, Yi Xia ^{2,*} and Chris Wolverton^{1,†}

¹*Department of Materials Science and Engineering, Northwestern University, Evanston, Illinois 60208, USA*

²*Department of Mechanical and Materials Engineering, Portland State University, Portland, Oregon 97201, USA*

 (Received 28 May 2023; revised 9 October 2023; accepted 16 November 2023; published 30 November 2023)

Accurate and reliable first-principles simulations of lattice thermal conductivity (κ_L) of highly anharmonic crystals have long been challenging in condensed matter and materials physics. With recent theoretical advances, the calculation of κ_L has evolved into a sophisticated process requiring the consideration of higher levels of refinements, such as high-order phonon-phonon scattering, anharmonic phonon renormalization, and heat transport beyond the phonon gas picture. Interatomic force constants (IFCs), however, as a shared pillar of the above concepts, are sometimes ambiguously implemented in this process, resulting in non-negligible uncertainties among different studies. Here, we revisit the ultralow κ_L of Tl_3VSe_4 and make a rigorous comparison of κ_L obtained from IFCs extracted by different approaches (flavors). We find that the fourth-order IFCs extracted with small-displacement data (0 K) are prone to yield significant phonon frequency shifting (phonon renormalization) and four-phonon scatterings, which lead to distinctively increased or decreased κ_L , respectively. Moreover, the different flavors of second-, third-, and fourth-order IFCs extracted with the same large-displacement data (temperature-dependent) also result in significantly disparate κ_L owing to the mixing of higher-order IFCs into the lower-order IFCs. Our work discloses the potential uncertainties of κ_L that arise from the choice of different flavors of IFCs and underscores the pressing need for more rigorous and robust approaches to extracting IFCs.

DOI: [10.1103/PhysRevB.108.184307](https://doi.org/10.1103/PhysRevB.108.184307)

I. INTRODUCTION

Crystals exhibiting strong anharmonicity, such as rock salts PbTe [1], PbSe [2], layered compounds SnSe [3] and BaSnS₂ [4], diamondlike compound AgGaTe₂ [5], and glasslike tetrahedrite Cu₁₂Sb₄S₁₃ [6], pose a formidable challenge to lattice dynamics studies. Prevalent weak bonds in these materials make the lattice vibrations substantially deviate from the harmonic picture, thus promoting phonon frequency shifting and phonon linewidth broadening at finite temperatures. These effects result in significant discrepancies between the lattice thermal conductivity (κ_L) values obtained by experimental measurements and first-principles calculations, including the lowest level of anharmonicity [harmonic approximation for phonon dispersion and three-phonon scattering for phonon lifetime (HA+3ph)] [7–11]. In order to address this inconsistency, extensive efforts have been made to develop an advanced lattice dynamics framework from first principles considering higher-order anharmonicity based on the perturbation theory [1,12–20]. By extending the Taylor expansion of force F_a felt by atom a beyond the second order (i.e., harmonic term), the anharmonicity can be captured by higher-order terms such as the third- and fourth-order terms:

$$F_a = -\Phi_{aa_1}^{(2)} u_{a_1} - \frac{1}{2!} \Phi_{aa_1 a_2}^{(3)} u_{a_1} u_{a_2} - \frac{1}{3!} \Phi_{aa_1 a_2 a_3}^{(4)} u_{a_1} u_{a_2} u_{a_3} \dots, \quad (1)$$

where $\Phi^{(i)}$ is the i th-order interatomic force constants (IFCs), and u is the atomic displacement. By including the third-order IFCs, one can account for three-phonon interactions, which have two types of effects: first, three-phonon scattering, which leads to finite phonon lifetime; and second, phonon frequency shifting, referred to as phonon renormalization. Accordingly, phonon linewidth broadening and frequency shifting induced by four-phonon interactions can be described by the fourth-order IFCs. On top of this, coherent phonon transport has been proposed [21] as an extra channel for heat conduction and a methodology for its incorporation has recently been demonstrated in calculating the κ_L of CsPbBr₃ [22] and Si [23].

Tl_3VSe_4 [24–27], a strongly anharmonic crystal under intensive investigation, is particularly suitable for showcasing how the above advanced theories help reduce the discrepancy between experimental and calculated results. Mukhopadhyay *et al.* [24] first calculated the κ_L of Tl_3VSe_4 to be 0.16 W m⁻¹ K⁻¹ at 300 K at the HA+3ph level of approximation, only half of the experimental value (0.30 W m⁻¹ K⁻¹). They subsequently added an extra κ_L contribution from short-mean-free-path phonons based on the Cahill-Watson-Pohl model [28], which brings the total κ_L to 0.368 W m⁻¹ K⁻¹. Xia *et al.* [25] later proposed that strong quartic anharmonicity plays a vital role in determining the κ_L of Tl_3VSe_4 . The calculated κ_L based on phonon-gas model (population phonon channel) with self-consistent phonon renormalization and three- and four-phonon scattering considered (SCPH+3, 4ph) reached 0.29 W m⁻¹ K⁻¹. The κ_L through coherent phonon transport channel was found to be relatively small, with a value of 0.08 W m⁻¹ K⁻¹ calculated in their work. Meanwhile, Jain

*yxia@pdx.edu

†c-wolverton@northwestern.edu

[26] calculated the population κ_L with the same level of approximation (SCPH+3, 4ph) but got a distinct result of $0.08 \text{ W m}^{-1} \text{ K}^{-1}$ accompanied by a much larger coherence κ_L of $0.15 \text{ W m}^{-1} \text{ K}^{-1}$. The most recent work by Zeng *et al.* [27] even goes beyond the perturbation theory. They recalculated the κ_L of Ti_3VSe_4 using the molecular dynamics simulation with a first-principles-based machine learning interatomic potential, which gives population κ_L and coherence κ_L of 0.13 and $0.16 \text{ W m}^{-1} \text{ K}^{-1}$, respectively. Their results suggest that anharmonicity up to the fourth order might still be inadequate to describe the lattice dynamics of Ti_3VSe_4 .

The aforementioned studies have revealed that as higher-order anharmonic terms are considered, the calculated κ_L will be distinctly different. However, it is worth noting that even with the same order of anharmonic terms included, disparities still exist in the results. For instance, the population κ_L at SCPH+3, 4ph level in Xia *et al.*'s [25] work is $0.29 \text{ W m}^{-1} \text{ K}^{-1}$, whereas Jain [26] got a significantly lower value of $0.08 \text{ W m}^{-1} \text{ K}^{-1}$. Apart from the most obvious differences due to exchange-correlation functionals, criteria of convergence test, potential energy surface sampling, force-fitting optimizers [29], etc., we recently found that different approaches of extracting IFCs (which we refer to as IFC flavors) would also lead to notable variances in calculated κ_L . The causes of the variances are subtle and nontrivial, and have not been systematically studied before.

We first categorize the most common IFCs extraction methods into two types: (i) the finite-displacement approach as implemented in PHONO3PY [30] or PHONOPY [31], THIRDDORDER.PY [32], and FOURTHORDER.PY [33] (generating second-order IFCs with DFPT method is considered aligned with this approach), and (ii) the force-fitting approach represented by compressive sensing lattice dynamics (CSLD) [34], temperature-dependent effective potential (TDEP) [35], stochastic self-consistent harmonic approximation (SSCHA) [36], or ALAMODE [18]. The former calculates IFCs as the derivatives of Eq. (1) using crystal structure configurations with small atomic displacement around the equilibrium position, thus leaving all IFCs intact and without renormalization from higher-order terms. We refer to these IFCs as bare IFCs. The latter, in contrast, uses crystal structure snapshots with larger atomic displacements, typically selected from *ab initio* molecular dynamics (AIMD) trajectories at finite temperatures. During the fitting process of Eq. (1), higher-order IFCs can mix into lower-order IFCs (similar with the aliasing problem in audio signal processing field [37–39]), which is considered as having the same effect as anharmonic phonon renormalization. The mixing can be further complicated due to the choice of different orders of precedence to fit each set of IFCs. Here we define five distinct flavors of IFCs based on differences in IFC extraction approaches and fitting sequences:

(1) When using the finite-displacement approach for extracting IFCs from the small-displacement data, the resulting IFCs are referred to as having a plain (pl) flavor.

(2) IFCs extracted from large-displacement data with the force-fitting approach can be further classified according to the fitting sequence.

(i) If the second-, third-, and fourth-order IFCs are fitted simultaneously, they are regarded as possessing a one-shot (os) flavor.

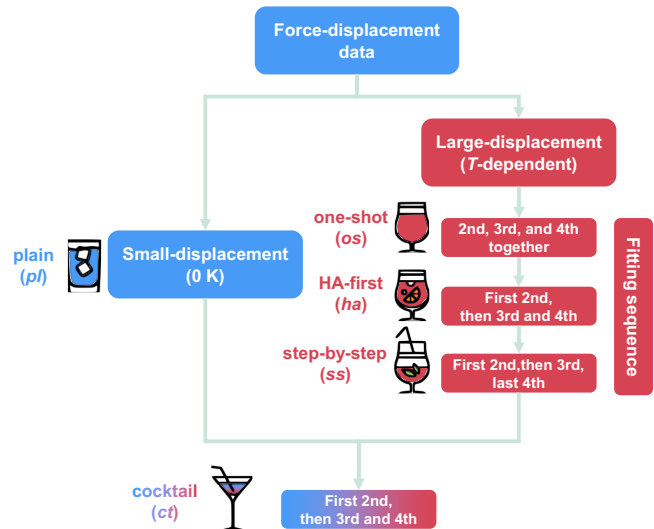


FIG. 1. Schematic of five flavors of interatomic force constants (IFCs): plain (pl), one-shot (os), harmonic-first (ha), step-by-step (ss), and cocktail (ct). The details of force-displacement data and fitting sequence for each flavor are given by side.

(ii) If the second-order IFCs are fitted first, and the third- and fourth-order IFCs are fitted together with the residual, these IFCs are characterized as having a harmonic-first (ha) flavor.

(iii) Or, if the third- and fourth-order IFCs are fitted separately and sequentially with the residual of previous terms, the IFCs are considered to have a step-by-step (ss) flavor.

(3) Eventually, there is another flavor of IFCs called cocktail (ct), which combines the second-order IFCs extracted with the finite-displacement approach and third- and fourth-order IFCs extracted with the force-fitting approach.

All the IFC flavors and their respective definitions are illustrated in Fig. 1. These IFCs with different flavors are widely used in a diverse selection of κ_L -calculation studies in the past five years. Some of them are classified according to IFC flavors and listed in Table I. As indicated in Table I, five different IFC flavors have been implemented in κ_L calculation of various compounds including rock salts [40], pyrites [41], perovskites [8], and clathrates [7,42]. Furthermore, multiple flavors of IFCs are utilized in calculating the κ_L of a single compound, i.e., Ti_3VSe_4 , which adds another layer of complexity when comparing the results of these works. Note that our study is not intended to judge the appropriateness of each IFC flavor, neither to directly compare the calculated κ_L values with experimental results. Clarification of the pros and cons of each IFC flavor is a highly nontrivial task, particularly due to the convolution of different orders of anharmonicity, which will be left for future research. Instead, here we focus on characterizing the differences in phonon spectra and κ_L resulted from the corresponding IFC flavors.

Here, we revisit the first-principles κ_L calculations of Ti_3VSe_4 with the state-of-the-art framework of perturbation theory, which includes the three- and four-phonon scattering, self-consistent phonon renormalization, and the two-channel phonon transport. Readers can refer to the Appendixes for

TABLE I. Collection of published κ_L studies, sorted by different flavors of IFCs used.

IFC flavor	Author	Codes	Year	Compound
plain	S. Mukhopadhyay <i>et al.</i> [24]	PHONOPY & PHONO3PY	2018	Tl ₃ VSe ₄
	T. Jia <i>et al.</i> [41]	PHONOPY & THIRDDORDER.PY	2020	ZnSe ₂
	T. Pandey <i>et al.</i> [43]	PHONOPY & PHONO3PY ^a	2020	TlBr
one-shot	L. Xie <i>et al.</i> [44]	TDEP ^b	2020	AgCrSe ₂
HA first	N. K. Ravichandran <i>et al.</i> [40]	In-house codes ^b	2018	NaCl
	A. Jain [26]	In-house codes ^b	2020	Tl ₃ VSe ₄
	T. Pandey <i>et al.</i> [43]	TDEP ^{a, b}	2020	TlBr
step-by-step	J. Klarbing <i>et al.</i> [45]	TDEP ^b	2020	Cs ₂ AgBiBr ₆
cocktail	T. Tadano <i>et al.</i> [7]	ALAMODE	2018	Ba ₈ Ga ₁₆ Ge ₃₀
	Y. Xia <i>et al.</i> [25]	CSLD	2020	Tl ₃ VSe ₄
	Q. Zhong <i>et al.</i> [46]	ALAMODE	2021	M ₃ Sb(M = K, Rb, Cs)
	Y. Zhao <i>et al.</i> [8]	ALAMODE	2021	Perovskites
	Y. Nishimura <i>et al.</i> [47]	ALAMODE	2022	(Pb _{1-x} Sn _x)Se
	M. Ohnishi <i>et al.</i> [42]	ALAMODE	2022	Ba ₈ Ga ₁₆ Sn ₃₀

^aThe authors performed a comparative study by using both flavors of IFCs.

^bThese studies generated the initial second-order IFCs as bare ones, but they fitted the final renormalized IFCs in a pure force-fitting approach.

details on the formalism of SCPH (Appendix B), the numerical evaluation of phonon scattering rates (Appendix C), and solving the Peierls-Boltzmann transport equation for two-channel κ_L (Appendix D). By enforcing all the conditions (except IFC flavors) to be the same when calculating κ_L , we systematically compare the impact of IFC flavors on phonon frequency and phonon linewidth. Results suggest that when calculating κ_L with pl flavor of IFCs, the fourth IFCs are highly sensitive to the displacing scheme and the displacement amplitude, and the pl flavor fourth IFCs tends to bring significant phonon mode hardening and phonon scattering. The other four flavors of IFCs induce the inevitable mixing of higher-order IFCs to lower-order IFCs, which also brings significant uncertainties of calculated κ_L . Our findings indicate the potential uncertainty when comparing the κ_L calculated with different flavors of IFCs, which highlights the need for a universal IFC-extraction method that is independent of fitting flavors in future lattice dynamics studies.

II. METHODOLOGY

A. Density functional theory (DFT) calculations

We used the Vienna *ab initio* simulation package (VASP) [48] to relax the atomic positions (lattice parameters fixed at 300 K experiment value of 7.71 Å [24]), obtain the energies and forces, and run AIMD simulations. The energy cutoff for plane-wave basis was 500 eV. We adopted an $8 \times 8 \times 8$ Γ -centered \mathbf{k} mesh to sample the Brillouin zone of the primitive cell. The Γ -centered \mathbf{k} mesh of the same density was used in subsequent calculations on supercells. We set a force and energy convergence criteria of 10^{-3} eV Å⁻¹ and 10^{-8} eV, respectively, for the structure relaxation and static calculation. The PBEsol [49] exchange-correlation functional was chosen based on our previous work [25].

B. Interatomic force constant (IFC) extraction

When extracting the second-order IFCs with pl and ct flavors, we utilized PHONOPY [31], which is implemented with

the finite-displacement approach. To balance the efficiency and accuracy, a $2 \times 2 \times 2$ supercell (64 atoms) was chosen based on our previous work [25]. We performed the nonanalytic correction of the phonon dispersion near the Brillouin zone center using the mixed-space approach [50], with macroscopic static dielectric constants and Born effective charges determined by density functional perturbation theory (DFPT) encoded in VASP [51,52]. The pl flavor third- and fourth-order IFCs were subsequently extracted from the same supercell by using THIRDDORDER.PY [32] and FOURTHORDER.PY [33] scripts, respectively. For those IFCs extracted with force-fitting approach (os, ha, ss, and ct flavors), we utilized CSLD [34] to perform the fitting. The force-displacement data were obtained from a collection of 100 snapshots, equally spaced in time, extracted from a 40 ps trajectory of an AIMD simulation on a $2 \times 2 \times 2$ supercell at 300 K. We tested the number of snapshots from 40–100, and found that calculated κ_L (SCPH+3, 4ph) converged within $\pm 5\%$ at 80 snapshots, which is consistent with the convention of previous Tl₃VSe₄ study using CSLD [25]. For both approaches, the cutoff radius for second-, third-, and fourth-order IFCs are tested to be converged at 10 Å, 7 Å, and 4 Å, respectively. Further details regarding the convergence test of cutoff radii are presented in Appendix A.

III. RESULTS AND DISCUSSIONS

A. Effects of displacement schemes and amplitudes

We first examined the impact of pl-flavor IFCs on κ_L , using three different displacement schemes and amplitudes. PHONOPY [31], THIRDDORDER.PY [32], and FOURTHORDER.PY [33] scripts were used to generate force-displacement structures by displacing one atom at a time with small displacements of 0.01 Å for second-order IFCs, and 0.03 Å for third- and fourth-order IFCs (denoted as Fourthorder group). CSLD [34] was also used to generate the force-displacement structures, but with a scheme that moves all the atoms towards a random direction at 0.01 Å for second-order IFCs,

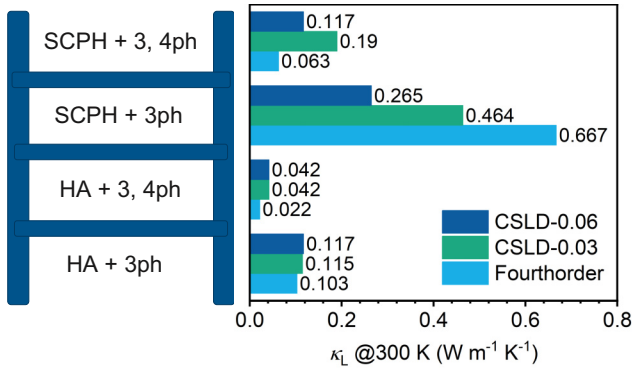


FIG. 2. Lattice thermal conductivity (κ_L) calculated with three different schemes (Fourthorder, CSLD-0.03, and CSLD-0.06) aligned with the increasing level of approximation. HA: harmonic approximation. SCPH: self-consistent phonon renormalization. 3, 4ph: three- and four-phonon scattering.

and 0.03 Å (CSLD-0.03 group) or 0.06 Å (CSLD-0.06 group) for third- and fourth-order IFCs. We selected up to 0.06 Å displacements as the reference group for internal comparisons of the pl flavor, since larger displacements such as 0.09 Å are already approaching the average atomic displacement of 0.1 Å in snapshots generated by AIMD simulations at 50 K, which might not be considered as small-displacement data.

Figure 2 shows the κ_L of Ti_3VSe_4 calculated at four different levels of approximation (HA+3ph, HA+3, 4ph, SCPH+3ph, and SCPH+3, 4ph) using the three groups of IFCs. The comparison of κ_L at a higher level of approximation (SCPH+3, 4ph+two-channel) is trivial and exhibited in Appendix D. As can be seen in Fig. 2, regardless of which group of IFCs are used, κ_L (3, 4ph) are always smaller than κ_L (3ph), whereas κ_L (SCPH) are always larger than κ_L (HA), which indicates the four-phonon scattering tends to decrease the κ_L , while SCPH tends to increase the κ_L by hardening the essential heat-carrying phonon modes of Ti_3VSe_4 . The three groups present similar κ_L at HA+3ph level, but soon show distinct values after including the effect of the fourth-order anharmonicity. The κ_L in Fourthorder group experiences the most pronounced influence. It shows approximately less than half of the value of the other two groups at HA+3, 4ph and SCPH+3, 4ph levels. Meanwhile, it is significantly larger than the other two groups at SCPH+3ph level. The large

κ_L variation among the three groups beyond the HA+3ph level of approximation hints at the underlying influence from the fourth-order IFCs.

To evaluate the influence from the fourth-order IFCs and beyond, we look into the temperature-dependent phonon dispersion [shown in Figs. 3(a)–3(c)] and four-phonon scattering rates [shown in Fig. 3(d)]. The Fourthorder group in Fig. 3(a) shows evident phonon hardening across the whole Brillouin zone at frequencies ranging from 0–125 cm^{-1} with increasing temperature, whereas the CSLD-0.03 group in Fig. 3(b) and the CSLD-0.06 group in Fig. 3(c) show only moderate phonon frequency shifts below 50 cm^{-1} . In Fig. 3(d), substantial four-phonon scattering rates are also observed in the Fourthorder groups at 300 K, nearly double the scattering rates of the CSLD-0.03 and CSLD-0.06 group across 0–125 cm^{-1} .

In summary, bare fourth-order IFCs of Ti_3VSe_4 calculated with the finite-displacement method (Fourthorder group) are prone to stiffen the phonon modes and strengthen the phonon scattering significantly. This effect could possibly be compromised by the renormalization of the fourth-order IFCs from higher-order anharmonic terms (from fifth-order to infinite-order) as observed in CSLD reference groups. This emphasizes the significant impact from higher-order anharmonicity on phonon dispersion and scattering rates. Furthermore, comparison between Fourthorder group (in which one atom is moved by 0.01/0.03 Å at a time) and CSLD-0.03 group (in which all atoms are moved by 0.01/0.03 Å at a time) indicates the potential impact of phonon mode correlations induced by the collective atomic displacement in the fitting data of the CSLD reference group. Even using the same atomic displacement scheme, in CSLD reference groups, one can obtain rather different renormalization effects using different amplitudes of displacements. As can be seen from Figs. 3(b) and 3(c), noticeable differences between phonon frequencies 0–25 cm^{-1} can be observed. In Fig. 3(d), this also leads to distinct phonon scattering rates between CSLD-0.03 and CSLD-0.06 groups around 25 cm^{-1} . The comparison between CSLD-0.03 and CSLD-0.06 group suggests that the fitting of high-order anharmonic terms is highly sensitive to the amplitude of atomic displacement.

B. Effects of fitting sequence

We now shift the focus to the influence of the fitting sequence on IFC extraction. Given that IFCs could substantially

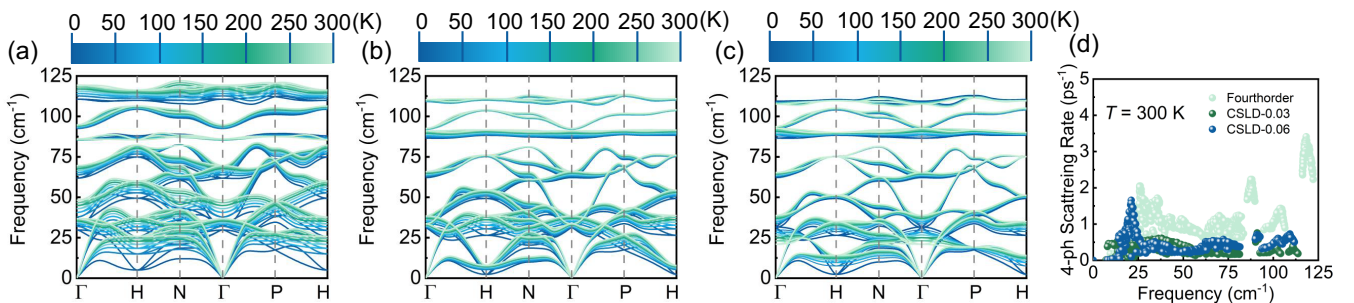


FIG. 3. Temperature-dependent phonon dispersion of (a) Fourthorder, (b) CSLD-0.03, and (c) CSLD-0.06 groups from $T = 0$ to 300 K (temperature implemented only in SCPH equation). (d) Four-phonon scattering rates of the three groups at 300 K and SCPH+3, 4ph level of approximation

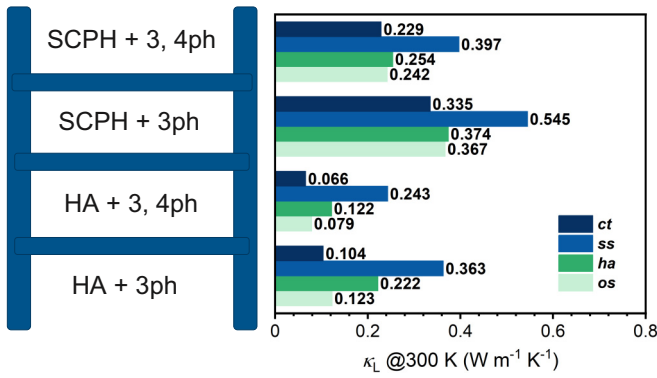


FIG. 4. (a) κ_L calculated with one-shot (os), HA-first (ha), step-by-step (ss), and cocktail (ct) flavors of IFCs, aligned with increasing level of approximation from HA+3ph to SCPH+3, 4ph.

vary with the displacement amplitude of the fitting data, we further explore the remaining four flavors (os, ha, ss, and ct) of IFCs extracted by CSLD using the same set of force-displacement data generated at 300 K by AIMD. As depicted in Fig. 4, each flavor has the same trend of calculated κ_L versus the level of approximation with that of pl flavor, i.e., κ_L (HA+3, 4ph) < κ_L (HA+3ph), κ_L (SCPH+3, 4ph) < κ_L (SCPH+3ph), and κ_L (HA) < κ_L (SCPH), which again emphasizes the importance of fourth-order anharmonicity in Ti_3VSe_4 . However, the detailed comparison of κ_L in Fig. 4 indicates a more sophisticated influence from the four IFC flavors. We list the main differences between the flavors as below:

- (1) κ_L (ss) is always the highest value at all levels of approximation.
- (2) κ_L (os) and κ_L (ha) show similar values at SCPH but distinct values at the HA approximation level.
- (3) κ_L (ct) is always the lowest value at all levels of approximation.

Based on the aforementioned analysis, the influence of different orders of IFCs on κ_L manifests intricate interactions. The determination of the sole influence stemming from individual IFC orders becomes challenging when the remaining orders of IFCs vary concurrently. To disentangle the effects of individual IFC order, we employ the control variates (CV) method, keeping fixed those IFC orders that are not the subject of our investigation. For example, when investigating the impact of the second-order IFC flavor, we hold the higher order IFCs (the third- and fourth-order) constant for each group, while using the second-order IFCs from each flavor. This ensures that any observed κ_L differences are solely attributed to the second-order IFCs with different flavors. According to our previous study [25], the fourth-order polynomial is assumed to adequately define the major features of the potential energy surface of Ti_3VSe_4 at 300 K. Based on this prerequisite, the os flavor IFCs tend to induce less mixing from higher-order IFCs during the fitting. Therefore, we choose the IFCs with the os flavor as the default setting and change the IFCs we want to study one at a time. Meanwhile, when investigating the κ_L differences resulting from the individual sets of IFCs, we adopt the HA+3, 4ph level of approximation to rule out the renormalization from the SCPH theory. The SCPH+3,

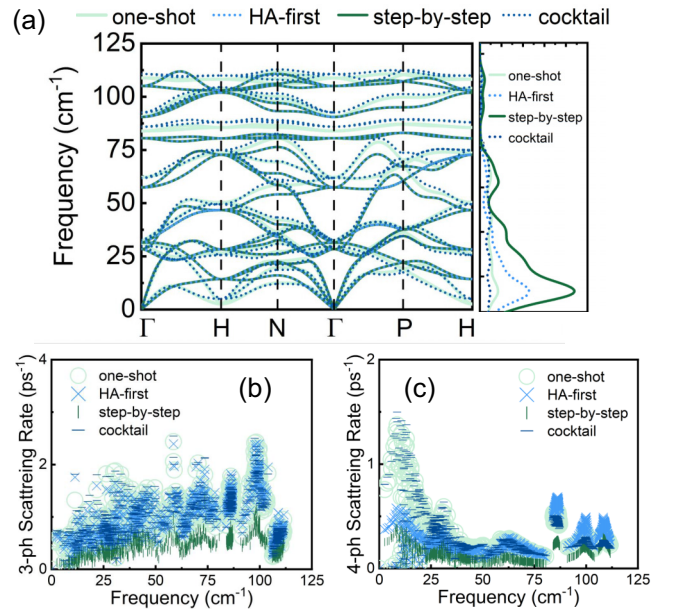


FIG. 5. (a) Left: Phonon dispersion of the four flavors converted from second-order IFCs without SCPH effect. Right: κ_L differential with respect to the phonon frequency. Higher values indicate higher κ_L contribution from phonon modes at this frequency. (b) Three-phonon scattering rates versus phonon frequency at the HA+3, 4ph level of approximation for four control variate (CV) groups. (c) Four-phonon scattering rates versus phonon frequency at the HA+3, 4ph level of approximation for four CV groups.

4ph level of approximation is used exclusively for the purpose of evaluating the renormalization effect of fourth-order IFCs. All the results are listed in Table II.

We first study the influence of second-order IFC flavors. Results in the first row of Table II suggest that κ_L^{CV} (os) and κ_L^{CV} (ct) are similar, while κ_L^{CV} (ha) and κ_L^{CV} (ss) (the two flavors have identical second-order IFCs) present values nearly twice as high as theirs. This result can be explained by the phonon κ_L contribution and phonon dispersions in Fig. 5(a). The right panel of Fig. 5(a) is generated by calculating the derivatives of accumulative κ_L with respect to the phonon frequency. A peak in this figure generally means major κ_L contribution from phonons at the corresponding frequencies. The left panel of Fig. 5(a) compares the phonon dispersions converted from the second-order IFCs with four different flavors. As suggested by the phonon κ_L -contribution curves, ha- and ss-flavor phonon modes with frequencies less than 25 cm^{-1} contribute most of the κ_L , whereas os- and ct-flavor phonons have more averaged κ_L contribution from phonon modes with frequencies ranging from 0–75 cm^{-1} . In the phonon frequency range of 0–25 cm^{-1} , ha and ss flavors produce harder phonon branches than os and ct flavors. One of the most extreme examples is, as shown in Fig. 5(a), that the acoustic phonon modes with ha and ss flavor show significantly higher frequency (14 cm^{-1}) than that with os and ct flavor (2 cm^{-1}) at the H point, which enhances the group velocity of neighboring phonon modes, and thus leads to a larger κ_L . This is due to the fitting sequence of the ha and ss flavors that results in higher-than-second-order terms mixing into the second-order terms when the second-order IFCs are fitted first,

TABLE II. κ_L at 300 K calculated with IFCs allocated by control variates (CV) method. Varied IFCs comes from each corresponding flavor, whereas fixed IFCs always come from the os flavor. The first three rows of κ_L are calculated at HA+3, 4ph level of approximation, and the last row of κ_L is calculated at SCPH+3, 4ph level of approximation.

	$\kappa_L(os)$ /Wm ⁻¹ K ⁻¹	$\kappa_L(ha)$ /Wm ⁻¹ K ⁻¹	$\kappa_L(ss)$ /Wm ⁻¹ K ⁻¹	$\kappa_L(ct)$ /Wm ⁻¹ K ⁻¹
second-order IFCs varied, third- and fourth-order IFCs fixed	0.079	0.138	0.138	0.069
third-order IFCs varied, second- and fourth-order IFCs fixed	0.079	0.081	0.142	0.077
fourth-order IFCs varied, second- and third-order IFCs fixed	0.079	0.087	0.097	0.077
Renorm. second-order IFCs varied, third- and fourth-order IFCs fixed	0.242	0.256	0.207	0.241

which can have an effect similar to that of renormalization. However, this is not the case when the second-order IFCs are calculated with the finite-displacement method (the ct flavor), or to a lesser extent when the second-order IFCs are fitted concurrently with third- and fourth-order IFCs (the os flavor).

The κ_L^{CV} calculated with varied flavors of third-order IFCs in the second row of Table II suggest that $\kappa_L^{CV}(os)$, $\kappa_L^{CV}(ct)$, and $\kappa_L^{CV}(ha)$ are similar. What stands out the most is the $\kappa_L^{CV}(ss)$, which again shows nearly double the value of others. The impact of third-order IFCs can be evaluated by three-phonon scattering rates, as depicted in Fig. 5(b). The ss-flavor third-order IFCs present significantly lower scattering rates across the whole phonon modes, whereas the other three show a similarly higher level of scattering rates. The results indicate a non-negligible amount of the higher-than-third-order IFCs might mix into the third-order IFCs during the fitting of ss-flavor IFCs, resulting in substantially weakened three-phonon scattering.

In the third row of Table II, although the trend of $\kappa_L^{CV}(ct) < \kappa_L^{CV}(os) < \kappa_L^{CV}(ha) < \kappa_L^{CV}(ss)$ is maintained, the calculated κ_L^{CV} with different flavors of fourth-order IFCs show less distinct values. Figure 5(c), on the one hand, shows that four-phonon scattering rates is overall smaller than three-phonon scattering rates, suggesting a nondominant role of four-phonon scattering. On the other hand, the scattering rates of the ha and ss flavors start approaching that of the os and ct flavors from the frequency of 12 cm⁻¹, leading to a smaller amount of the κ_L difference arising from four-phonon scattering rates. However, the influence of fourth-order-IFC flavors is manifested not only in four-phonon scattering but

also in the renormalization based on SCPH theory. We plot the temperature-dependent phonon dispersion of the four IFC flavors in Fig. 6 to illustrate the effect of renormalization. Figures 6(a) and 6(d) show that low-frequency phonon branches (<25 cm⁻¹) with os and ct flavors present pronounced hardening with increasing temperature. On the contrary, phonon branches with the ha and ss flavors in Figs. 6(b) and 6(c) display insignificant hardening at low frequencies, but evident hardening at high frequencies (>25 cm⁻¹). Compared with the os and ct flavors, the insignificant hardening of low-frequency and significantly hardening of high-frequency phonon branches of ha and ss flavors in Figs. 6(b) and 6(c) are tangled with their prehardened low-frequency and presoftened high-frequency phonon branches before the implementation of SCPH as shown in Fig. 5(a), respectively. This is because when fitting second-order IFCs individually with ha and ss flavors, we already have part of the fourth-order IFCs mixed into the second-order IFCs and prenormalized it before solving the SCPH equation.

To give a conclusive evaluation of the renormalization based on SCPH theory, we also calculate the κ_L at 300 K at the SCPH+3, 4ph level of approximation with only the renormalized second-order IFCs changing. The results in the last row of Table II show that κ_L^{CV} calculated with ss-flavor renormalized second-IFCs is the lowest due to the most insignificant low-frequency phonon hardening observed in Fig. 6(c). We attribute the phenomenon to the weakened renormalization ability of ss-flavor fourth-order IFCs. This, in combination with the weaker four-phonon scattering rates previously depicted in Fig. 5(c), suggests an overall weakened ability (both

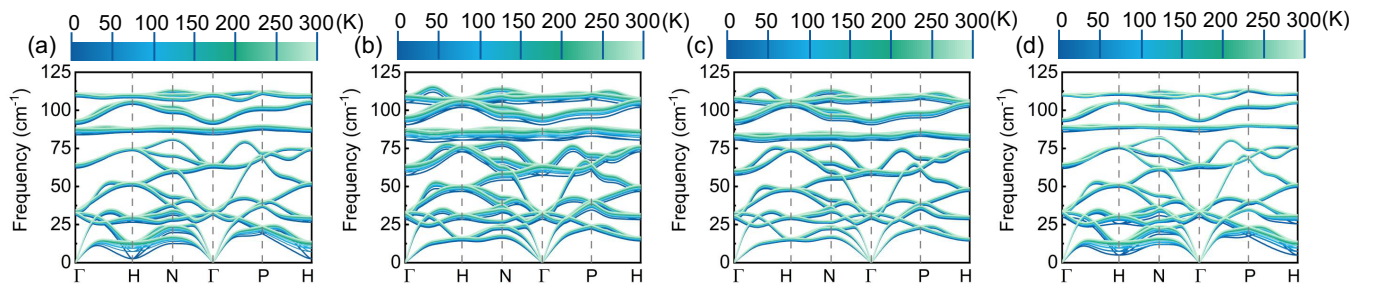


FIG. 6. Temperature-dependent phonon dispersion of (a) one-shot (os), (b) HA-first (ha), (c) step-by-step (ss), and (d) cocktail (ct) flavors from $T = 0$ to 300 K (temperature implemented only in SCPH equation).

renormalization and scattering) of ss-flavor fourth-order IFCs. This weakening is linked to the aforementioned mixing of higher-than-third-order terms into the third-order terms of ss flavor, which leaves less residual for fitting the fourth-order terms. Other three flavors of renormalized second IFCs yield similar κ_L^{CV} with the highest value goes to κ_L^{CV} (ha), which suggests an overall stronger renormalization with ha flavor as is also observed in Fig. 6(b).

Through the CV analysis above, we can again list the origin of the main differences between κ_L calculated with different flavors of IFCs:

(1) When fitting the IFCs with the ss flavor, the mixing of the higher-order IFCs into the third-order IFCs results in significantly weakened three-phonon scattering, which is the dominant factor leading to κ_L (ss) higher than others.

(2) The mixing of the third- and fourth-order IFCs into the second-order IFCs might be substantially neutralized when considering four-phonon scattering and SCPH simultaneously, which contributes to less different κ_L (os) and κ_L (ha) at SCPH than at HA approximation level.

(3) Pure force-fitting flavors (os, ha, and ss) of IFCs have more or less higher-order IFCs mixing into the second-order IFCs, which serves as a prenormalization of bare second-order IFCs before SCPH. This effect, if not appropriately separated from SCPH, may result in the double counting of anharmonic renormalization, leading to a larger value than κ_L (ct), which is evaluated by bare second-order IFCs.

IV. CONCLUSION

In summary, we have performed a systematic investigation of the impact of five different IFC flavors on the calculated κ_L of Ti_3VSe_4 , which explicitly reveals the features of each flavor. The pl-flavor IFCs extracted with the finite-displacement method are bare with no mixing from higher-order anharmonicity. They tend to present significantly varied κ_L after including the four-phonon scattering and SCPH, which is possibly due to the lack of consideration of higher-than-fourth-order anharmonicity. The pure force-fitting flavors, namely the os, ha, and ss ones, have higher-order IFCs mixed into and prenormalize the second-order IFCs, which gives a higher estimation of κ_L than the ct flavor with bare second-order IFCs. For the ha and ss flavors, the mixing of third- and fourth-order IFCs into the second-order IFCs can be compromised by considering the SCPH and four-phonon scattering simultaneously, whereas the significantly weakened third-order IFCs that solely exist in the ss-flavor IFCs can still lead to significantly larger κ_L . We assume the relative magnitude of κ_L with different IFC flavors should be highly system dependent, but the uncertainties induced by using different flavors of IFCs substantially exist. Our study prompts caution for choosing and using these different flavors of IFCs and the pressing need for a more rigorous and robust fitting method of IFCs at finite temperatures for future studies of lattice dynamics.

ACKNOWLEDGMENTS

Z.L. and C.W. acknowledge the support from the Center for Hierarchical Materials Design (CHiMaD) under the

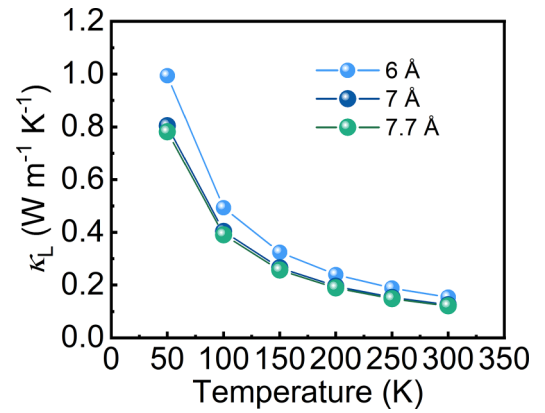


FIG. 7. Temperature-dependent κ_L (HA+3ph) calculated with os-flavor IFCs. The third-order IFCs with cutoff radii of 6 Å, 7 Å, and 7.7 Å were tested, while the second- and fourth-order IFC cutoff radii fixed at 10 Å and 4 Å, respectively.

Award No. 70NANB14H012 by U.S. Department of Commerce. Y.X. acknowledges Portland State University Lab Setup Fund. This work used the computational resource of Bridges-2 supercomputer at Pittsburgh Supercomputer Center (PSC) under Grant No. DMR160112 and Quest High Performance Computing Facility at Northwestern University. Y.X. acknowledges partial support from the US National Science Foundation through Award No. 2317008.

APPENDIX A: INTERATOMIC FORCE CONSTANT CUTOFF RADII

Given the intricate interplay between different orders of interatomic force constant (IFC) across different IFC flavors, a rigorous convergence test of IFC cutoff radii was supposed to be performed for each flavor separately and following the according fitting sequence. However, the computational demands for such an endeavor can be overwhelming. Given that os flavor requires the least interference and is thus less biased, We determined a set of cutoff radii using the os flavor and used them when extracting the other four flavors of IFCs. For the second-order IFCs, we set a sufficiently large cutoff radius of 10 Å, which covers the longest distance between any two atoms in a $2 \times 2 \times 2$ supercell of Ti_3VSe_4 (measured to be 7.7 Å). Beyond this distance, pair interactions are considered unphysical and are automatically excluded. Regarding the third- and fourth-order IFCs, we conducted a convergence test of κ_L with different cutoff radii. Due to the limited computational capacity, we performed the κ_L calculation only at HA+3ph level of approximation. We fixed the fourth-order IFC cutoff radius at 4 Å as was done in all previous Ti_3VSe_4 studies [25–27]. Figure 7 demonstrates that κ_L varied within 5% when increasing the third-order IFC cutoff radius from 7 Å–7.7 Å, providing evidence of convergence for the third-order IFCs at a cutoff radius of 7 Å. Our conclusion about the κ_L uncertainties arising from different IFC flavors should be considered as self-consistent within these unified cutoff radii.

APPENDIX B: SELF-CONSISTENT PHONON (SCPH) APPROXIMATION

In SCPH theory, the anharmonic phonon dispersion at finite temperature can be obtained by adding the first-order correction to the harmonic phonon frequency, which accounts for quartic anharmonicity [15,16]. The SCPH equation in the diagonal form is

$$\Omega_\theta^2 = \omega_\theta^2 + 2\Omega_\theta I_\theta, \quad (\text{B1})$$

where θ is a composite index for phonon mode with wave vector \mathbf{q} and on the s th phonon branch. ω is the harmonic phonon frequency, and Ω is the corresponding renormalized phonon frequency. The quantity I_θ can be defined as

$$I_\theta = \frac{\hbar}{8N} \sum_{\theta'} \frac{V^{(4)}(\theta, -\theta, \theta', -\theta')}{\Omega_\theta \Omega_{\theta'}} [1 + 2n(\Omega_{\theta'})], \quad (\text{B2})$$

where \hbar , N , $V^{(4)}$, and n are the reduced Planck constant, the number of sampled wave vectors, the reciprocal representation of the fourth-order IFCs, and the phonon population. Because phonon population obeys the Bose-Einstein distribution, the Eq. (B1) and Eq. (B1) are temperature dependent. We sampled the reciprocal space with a \mathbf{q} mesh of $2 \times 2 \times 2$ and solved SCPH equation self-consistently by iterating Eq. (B1) and Eq. (B2) with fixed fourth-order IFCs at corresponding temperature until a convergence criterion $\Delta\Omega$ of 10^{-4} meV is reached. As previous studies [1,7,53] have shown, the second-order correction to Ω from the cubic anharmonicity is negligible compared to the first-order correction. Therefore, we omitted it from this study.

APPENDIX C: THREE- AND FOUR-PHONON SCATTERING RATES

Based on the single-mode relaxation time approximation (SMRTA), the three- ($\tau_{3\text{ph},\theta}^{-1}$) and four-phonon ($\tau_{4\text{ph},\theta}^{-1}$) scattering rates can be expressed as [19]:

$$\tau_{3\text{ph},\theta}^{-1} = \sum_{\theta_1\theta_2} \left[\frac{1}{2} (1 + n_{\theta_1}^0 + n_{\theta_2}^0) \zeta_- + (n_{\theta_1}^0 - n_{\theta_2}^0) \zeta_+ \right], \quad (\text{C1})$$

$$\tau_{4\text{ph},\theta}^{-1} = \sum_{\theta_1\theta_2\theta_3} \left[\frac{1}{6} \frac{n_{\theta_1}^0 n_{\theta_2}^0 n_{\theta_3}^0}{n_\theta^0} \zeta_{--} + \frac{1}{2} \frac{(1 + n_{\theta_1}^0) n_{\theta_2}^0 n_{\theta_3}^0}{n_\theta^0} \zeta_{+-} + \frac{1}{2} \frac{(1 + n_{\theta_1}^0)(1 + n_{\theta_2}^0) n_{\theta_3}^0}{n_\theta^0} \zeta_{++} \right], \quad (\text{C2})$$

where the three-phonon scattering rates of the absorption (+) and emission (−) process can be further expressed as:

$$\zeta_\pm = \frac{\pi \hbar}{4N} |V^{(3)}(\theta, \pm\theta_1, -\theta_2)|^2 \Delta_\pm \frac{\delta(\omega_\theta \pm \omega_{\theta_1} - \omega_{\theta_2})}{\omega_\theta \omega_{\theta_1} \omega_{\theta_2}}, \quad (\text{C3})$$

and the four-phonon scattering rates of recombination (++) , redistribution (+−) , and splitting (−−) process are calculated by [ω in Eq. (C3) and Eq. (C4) can be substituted by Ω at SCPH level of approximation]

$$\zeta_{\pm\pm} = \frac{\pi \hbar^2}{8N^2} |V^{(4)}(\theta, \pm\theta_1, \pm\theta_2, -\theta_3)|^2 \Delta_{\pm\pm} \times \frac{\delta(\omega_\theta \pm \omega_{\theta_1} \pm \omega_{\theta_2} - \omega_{\theta_3})}{\omega_\theta \omega_{\theta_1} \omega_{\theta_2} \omega_{\theta_3}}, \quad (\text{C4})$$

where the reciprocal representation of the third- ($V^{(3)}$) and fourth-order IFCs ($V^{(4)}$) are

$$V^{(3)}(\theta, \pm\theta_1, -\theta_2) = \sum_{a,p_1a_1,p_2a_2} \sum_{\alpha\alpha_1\alpha_2} e^{\theta} \frac{e^{\pm\theta_1} e^{-\theta_2}}{\sqrt{m_a m_{a_1} m_{a_2}}} e^{\pm i\mathbf{q}_1 \cdot \mathbf{r}_{p_1}} e^{-i\mathbf{q}_2 \cdot \mathbf{r}_{p_2}}, \quad (\text{C5})$$

and

$$V^{(4)}(\theta, \pm\theta_1, \pm\theta_2, -\theta_3) = \sum_{a,p_1a_1,p_2a_2,p_3a_3} \sum_{\alpha\alpha_1\alpha_2\alpha_3} e^{\theta} \frac{e^{\pm\theta_1} e^{\pm\theta_2} e^{-\theta_3}}{\sqrt{m_a m_{a_1} m_{a_2} m_{a_3}}} e^{\pm i\mathbf{q}_1 \cdot \mathbf{r}_{p_1}} e^{\pm i\mathbf{q}_2 \cdot \mathbf{r}_{p_2}} e^{-i\mathbf{q}_3 \cdot \mathbf{r}_{p_3}}, \quad (\text{C6})$$

where p , a , and α index to the primitive cell, basis atoms, and Cartesian coordinate, respectively. m and \mathbf{r} represent the atomic mass and the lattice vector of primitive cell, respectively. \mathbf{q} , n^0 , and e denote the wave vector, equilibrium occupation number, and eigenvector of phonon mode, respectively. The momentum conservation was strictly enforced by $\Delta_\pm \equiv \delta(\mathbf{q} \pm \mathbf{q}_1 - \mathbf{q}_2)$ and $\Delta_{\pm\pm} \equiv \delta(\mathbf{q} \pm \mathbf{q}_1 \pm \mathbf{q}_2 - \mathbf{q}_3)$, and the energy conservation was enforced by a δ function approximated by adaptive Gaussian smearing [54] for $\tau_{3\text{ph},\theta}^{-1}$ and regular Gaussian smearing [32] for $\tau_{4\text{ph},\theta}^{-1}$.

APPENDIX D: LATTICE THERMAL CONDUCTIVITY BASED ON THE TWO-CHANNEL MODEL

The population part of lattice thermal conductivity (κ_L) was calculated by solving the Peierls-Boltzmann transport equation (PBTE) [55] iteratively under the single-mode relaxation time approximation (SMRTA) [32] as:

$$\kappa_L = \frac{1}{\Lambda N k_B T^2} = \sum_{\theta} (\hbar \omega_\theta)^2 n_\theta (n_\theta + 1) v_\theta \otimes v_\theta \tau_\theta, \quad (\text{D1})$$

where Λ , k_B , and T are the volume of primitive cell, Boltzmann constant, and absolute temperature, respectively. The coherent lattice thermal conductivity κ_L^c is computed using our in-house implementation [56,57] based on SMRTA [ω in Eq. (D1) and Eq. (D2) can be substituted by Ω at SCPH level of approximation]:

$$\kappa_L^c = \frac{\hbar^2}{\Lambda N k_B T^2} \sum_{\mathbf{q}} \sum_{s \neq s'} \frac{\omega_{\mathbf{q}}^s + \omega_{\mathbf{q}}^{s'}}{2} v_{\mathbf{q}}^{s,s'} \otimes v_{\mathbf{q}}^{s',s} \times \frac{\omega_{\mathbf{q}}^s n_{\mathbf{q}}^s (n_{\mathbf{q}}^s + 1) + \omega_{\mathbf{q}}^{s'} n_{\mathbf{q}}^{s'} (n_{\mathbf{q}}^{s'} + 1)}{4(\omega_{\mathbf{q}}^{s'} - \omega_{\mathbf{q}}^s)^2 + (\tau_{s,\mathbf{q}}^{-1} + \tau_{s',\mathbf{q}}^{-1})^2} (\tau_{s,\mathbf{q}}^{-1} + \tau_{s',\mathbf{q}}^{-1}), \quad (\text{D2})$$

where $\mathbf{v}_{\mathbf{q}}^{s,s'}$ is the generalized group velocity tensors calculated as [22,58]

$$\mathbf{v}_{\mathbf{q}}^{s,s'} = \frac{i}{\omega_{\mathbf{q}}^s + \omega_{\mathbf{q}}^{s'}} \sum_{\alpha,\beta} \sum_{m,p,q} e_{\mathbf{q}}^s(\alpha, p) D_{\beta\alpha}^{pq}(0, m) \times (\mathbf{R}_m + \mathbf{R}_{pq}) e^{i\mathbf{q} \cdot \mathbf{R}_m} e_{\mathbf{q}}^{s'}(\beta, q). \quad (\text{D3})$$

TABLE III. Population lattice thermal conductivity κ_L , coherence lattice thermal conductivity κ_L^c and total lattice thermal conductivity κ_L^{total} calculated with five different flavors of IFCs at SCPH+3, 4ph level of approximation.

(W m ⁻¹ K ⁻¹)	pl						ct
	I ^a	II ^a	III ^a	os	ha	ss	
κ_L	0.063	0.190	0.117	0.242	0.254	0.397	0.216
κ_L^c	0.086	0.080	0.067	0.062	0.070	0.052	0.078
κ_L^{total}	0.149	0.270	0.184	0.304	0.324	0.449	0.294

^aI for Fourthorder, II for CSLD-0.03, and III for CSLD-0.06.

Here, e , D , and \mathbf{R} denote the polarization vector, the dynamical matrix, and the lattice vector, respectively. α/β , m , and p/q are indices labeling the Cartesian coordinate, the unit cell, and the atoms within the unit cell.

The total relaxation time was determined following Matthiessen's rule as $\tau_\theta^{-1} = \tau_{3\text{ph},\theta}^{-1} + \tau_{4\text{ph},\theta}^{-1}$. We adopted a $16 \times 16 \times 16$ \mathbf{q} mesh for κ_L calculations involving three-phonon scattering process and a $12 \times 12 \times 12$ \mathbf{q} mesh for those involving three- and four-phonon scattering process, which remained consistent with our previous work [25]. The coherence lattice thermal conductivity κ_L^c and total lattice thermal conductivity $\kappa_L^{\text{total}} = \kappa_L + \kappa_L^c$ we calculated based on SCPH+3, 4ph level of approximation are listed at Table III along with the population lattice thermal conductivity κ_L . As is obviously indicated by Table III, κ_L^{total} has exactly the same trend with κ_L because the variation induced by κ_L^c is still rooted in the group velocity $v_{\mathbf{q}}^{s,s'}$ and phonon scattering rates $\tau_{s,\mathbf{q}}^{-1}$ used in Eq. (D2). Therefore, the origin of κ_L^{total} variation is consistent with that of κ_L variation and will not be repeated here.

- [1] Y. Xia, *Appl. Phys. Lett.* **113**, 073901 (2018).
- [2] Z. Tian, J. Garg, K. Esfarjani, T. Shiga, J. Shiomi, and G. Chen, *Phys. Rev. B* **85**, 184303 (2012).
- [3] T. Lanigan-Atkins, S. Yang, J. L. Niedziela, D. Bansal, A. F. May, A. A. Puretzy, J. Y. Lin, D. M. Pajeroski, T. Hong, S. Chi, G. Ehlers, and O. Delaire, *Nature Commun.* **11**, 4430 (2020).
- [4] Z. Li, H. Xie, S. Hao, Y. Xia, X. Su, M. G. Kanatzidis, C. Wolverton, and X. Tang, *Phys. Rev. B* **104**, 245209 (2021).
- [5] H. Xie, E. S. Bozin, Z. Li, M. Abeykoon, S. Banerjee, J. P. Male, G. J. Snyder, C. Wolverton, S. J. L. Billinge, and M. G. Kanatzidis, *Adv. Mater.* **34**, 2202255 (2022).
- [6] Y. Xia, V. Ozoliņš, and C. Wolverton, *Phys. Rev. Lett.* **125**, 085901 (2020).
- [7] T. Tadano and S. Tsuneyuki, *Phys. Rev. Lett.* **120**, 105901 (2018).
- [8] Y. Zhao, S. Zeng, G. Li, C. Lian, Z. Dai, S. Meng, and J. Ni, *Phys. Rev. B* **104**, 224304 (2021).
- [9] Y. Xia, V. I. Hegde, K. Pal, X. Hua, D. Gaines, S. Patel, J. He, M. Aykol, and C. Wolverton, *Phys. Rev. X* **10**, 041029 (2020).
- [10] C. Wang, Q. Wang, Q. Zhang, C. Chen, and Y. Chen, *Chem. Mater.* **34**, 7837 (2022).
- [11] Y. Li, J. Liu, and J. Hong, *Phys. Rev. B* **106**, 094317 (2022).
- [12] A. A. Maradudin and A. E. Fein, *Phys. Rev.* **128**, 2589 (1962).
- [13] R. A. Cowley, *Rep. Prog. Phys.* **31**, 123 (1968).
- [14] N. R. Werthamer, *Phys. Rev. B* **1**, 572 (1970).
- [15] I. Errea, B. Rousseau, and A. Bergara, *Phys. Rev. Lett.* **106**, 165501 (2011).
- [16] T. Tadano and S. Tsuneyuki, *Phys. Rev. B* **92**, 054301 (2015).
- [17] S. Narasimhan and D. Vanderbilt, *Phys. Rev. B* **43**, 4541 (1991).
- [18] T. Tadano, Y. Gohda, and S. Tsuneyuki, *J. Phys.: Condens. Matter* **26**, 225402 (2014).
- [19] T. Feng and X. Ruan, *Phys. Rev. B* **93**, 045202 (2016).
- [20] G. A. S. Ribeiro, L. Paulatto, R. Bianco, I. Errea, F. Mauri, and M. Calandra, *Phys. Rev. B* **97**, 014306 (2018).
- [21] P. B. Allen and J. L. Feldman, *Phys. Rev. Lett.* **62**, 645 (1989).
- [22] M. Simoncelli, N. Marzari, and F. Mauri, *Nature Phys.* **15**, 809 (2019).
- [23] L. Isaeva, G. Barbalinardo, D. Donadio, and S. Baroni, *Nature Commun.* **10**, 3853 (2019).
- [24] S. Mukhopadhyay, D. S. Parker, B. C. Sales, A. A. Puretzy, M. A. McGuire, and L. Lindsay, *Science* **360**, 1455 (2018).
- [25] Y. Xia, K. Pal, J. He, V. Ozoliņš, and C. Wolverton, *Phys. Rev. Lett.* **124**, 065901 (2020).
- [26] A. Jain, *Phys. Rev. B* **102**, 201201(R) (2020).
- [27] Z. Zeng, C. Zhang, Y. Xia, Z. Fan, C. Wolverton, and Y. Chen, *Phys. Rev. B* **103**, 224307 (2021).
- [28] D. G. Cahill, S. K. Watson, and R. O. Pohl, *Phys. Rev. B* **46**, 6131 (1992).
- [29] E. Fransson, F. Eriksson, and P. Erhart, *npj Comput. Mater.* **6**, 135 (2020).
- [30] A. Togo, L. Chaput, and I. Tanaka, *Phys. Rev. B* **91**, 094306 (2015).
- [31] A. Togo and I. Tanaka, *Scr. Mater.* **108**, 1 (2015).
- [32] W. Li, J. Carrete, N. A. Katcho, and N. Mingo, *Comput. Phys. Commun.* **185**, 1747 (2014).
- [33] Z. Han, X. Yang, W. Li, T. Feng, and X. Ruan, *Comput. Phys. Commun.* **270**, 108179 (2022).
- [34] F. Zhou, W. Nielson, Y. Xia, and V. Ozoliņš, *Phys. Rev. Lett.* **113**, 185501 (2014).
- [35] O. Hellman, P. Steneteg, I. A. Abrikosov, and S. I. Simak, *Phys. Rev. B* **87**, 104111 (2013).
- [36] I. Errea, M. Calandra, and F. Mauri, *Phys. Rev. B* **89**, 064302 (2014).
- [37] V. Valimäki and A. Huovilainen, *IEEE Signal Process. Mag.* **24**, 116 (2007).
- [38] H.-M. Lehtonen, J. Pekonen, and V. Välimäki, *J. Acoust. Soc. Am.* **132**, 2721 (2012).
- [39] J. D. Parker, V. Zavalishin, and E. Le Bivic, in *Proc. Int. Conf. Digital Audio Effects (DAFx-16)*, Brno, Czech Republic, 2016, pp. 137–144.
- [40] N. K. Ravichandran and D. Broido, *Phys. Rev. B* **98**, 085205 (2018).
- [41] T. Jia, J. Carrete, Z. Feng, S. Guo, Y. Zhang, and G. K. H. Madsen, *Phys. Rev. B* **102**, 125204 (2020).
- [42] M. Ohnishi, T. Tadano, S. Tsuneyuki, and J. Shiomi, *Phys. Rev. B* **106**, 024303 (2022).
- [43] T. Pandey, L. Lindsay, B. C. Sales, and D. S. Parker, *Phys. Rev. Mater.* **4**, 045403 (2020).

- [44] L. Xie, J. H. Feng, R. Li, and J. Q. He, *Phys. Rev. Lett.* **125**, 245901 (2020).
- [45] J. Klarbring, O. Hellman, I. A. Abrikosov, and S. I. Simak, *Phys. Rev. Lett.* **125**, 045701 (2020).
- [46] Q. Zhong, Z. Dai, W. Wang, Y. Zhao, and S. Meng, *Int. J. Energy Res.* **45**, 6958 (2021).
- [47] Y. Nishimura, X. He, T. Katase, T. Tadano, K. Ide, S. Kitani, K. Hanzawa, S. Ueda, H. Hiramatsu, H. Kawaji, H. Hosono, and T. Kamiya, *Adv. Electron. Mater.* **8**, 2200024 (2022).
- [48] G. Kresse and J. Furthmüller, *Comput. Mater. Sci.* **6**, 15 (1996).
- [49] J. P. Perdew, A. Ruzsinszky, G. I. Csonka, O. A. Vydrov, G. E. Scuseria, L. A. Constantin, X. Zhou, and K. Burke, *Phys. Rev. Lett.* **100**, 136406 (2008).
- [50] Y. Wang, J. J. Wang, W. Y. Wang, Z. G. Mei, S. L. Shang, L. Q. Chen, and Z. K. Liu, *J. Phys.: Condens. Matter* **22**, 202201 (2010).
- [51] S. Baroni and R. Resta, *Phys. Rev. B* **33**, 7017 (1986).
- [52] M. Gajdoš, K. Hummer, G. Kresse, J. Furthmüller, and F. Bechstedt, *Phys. Rev. B* **73**, 045112 (2006).
- [53] T. Feng, X. Yang, and X. Ruan, *J. Appl. Phys.* **124**, 145101 (2018).
- [54] W. Li, L. Lindsay, D. A. Broido, D. A. Stewart, and N. Mingo, *Phys. Rev. B* **86**, 174307 (2012).
- [55] R. E. Peierls, *Quantum Theory of Solids* (Oxford University Press, Oxford, 2001).
- [56] Y. Xia, D. Gaines, J. He, K. Pal, Z. Li, M. G. Kanatzidis, V. Ozoliņš, and C. Wolverton, A Unified Understanding of Minimum Lattice Thermal Conductivity, 08-09-2023, <https://github.com/yimavxia/minikappa>.
- [57] Y. Xia, D. Gaines, J. He, K. Pal, Z. Li, M. G. Kanatzidis, V. Ozoliņš, and C. Wolverton, *Proc. Natl. Acad. Sci.* **120**, e2302541120 (2023).
- [58] P. B. Allen and J. L. Feldman, *Phys. Rev. B* **48**, 12581 (1993).